48TH TURBOMACHINERY & 35TH PUMP SYMPOSIA
HOUSTON, TEXAS | SEPTEMBER 9-12, 2019
GEORGE R. BROWN CONVENTION CENTER

INTRODUCTION TO SCC FAILURES IN STEAM TURBINES AND SOLUTIONS

Kenichi Nishiyama
Engineer, Turbine Engineering & Design Section
Mitsubishi Heavy Industries Compressor Corporation
Hiroshima, Japan

Rishav Jain
Engineer, Turbine Engineering & Design Section
Mitsubishi Heavy Industries Compressor Corporation
Hiroshima, Japan

Kenichi Nishiyama is Engineer, Turbine Engineering & Design Section, Mitsubishi Heavy Industries Compressor Corporation, Hiroshima, Japan. He has 7 years of experience as a turbine engineer. Mr. Nishiyama graduated from Tokuyama College of Technology (Mechanical & Electrical Engineering).

Rishav Jain is Engineer, Turbine Engineering & Design Section, Mitsubishi Heavy Industries Compressor Corporation, Hiroshima, Japan. He has 2 year experience as a turbine engineer. Mr. Jain has B.Tech degree in Mechanical Engineering from Indian Institute of Technology (IIT), Kanpur, India.

ABSTRACT

Mechanical drive steam turbines play an important role in petro-chemical plants, and these turbines are protected for safe operation by number of monitoring and protection systems. Despite this, steam turbines can still be damaged due to a variety of insidious mechanisms. This paper introduces one of the major damage mechanisms affecting steam turbines, Stress Corrosion Cracking (SCC), along with steam cycle design (rotor life time evaluation) and effective countermeasures for SCC.

SCC has been a serious issue for many years affecting all steam turbine rotors which operates in wet steam region. In wet steam, chemical components such as sodium, potassium and chlorides can deposit in the gap between rotor and rotor disc due to insufficient water control for steam.

SCC is the result of a combination of three factors, - a susceptible material, exposure to a corrosive environment, and tensile stresses. In term of each factors, countermeasures for SCC on turbine blade disc has been studied and developed for decades and detail examples are shown in this paper along with actual experience (Reduction of working stress, developing of new material, elimination of corrosive substances etc). Case history is described for industrial turbine with descriptions of root causes and solutions. It is recommended that rotors be examined for signs of SCC damage by Phased Array Ultrasonic Test (PAUT) to mitigate the risk of SCC failure. Along with this technology, residual life estimations can be made based on the guidelines specified by the Electric Power Research Institute (EPRI) if cracks are detected.

INTRODUCTION

In petrochemical plants, steam often contains a small amount of corrosive chemicals which may result in corrosion-related problems such as stress corrosion cracking (SCC). SCC is one of the most insidious forms of corrosion damage for steam turbines because it often goes undetected until catastrophic failure occurs. First, an example of blade root failure will be introduced and the failure analysis methodology will be explained.

Second, in order to prevent such a failure, it is important to accurately estimate the residual life of a rotor. Although a EPRI has several published methods to predict the remaining life of a rotor, the crack propogation rate due to SCC highly depends on the rotor material. Therefore, crack growth rate were determined by conducting SCC growth tests under similar condition based on particular low alloy rotor material (Ni-1.25Cr-Mo-V forged steel) to establish a more accurate method using the test result. This paper also highlights the development of criteria to evaluate SCC growth rates of steam turbine blades.

Finally, when the life of the rotor has been exceeded, the end user has the option to replace the rotor entirely, or weld repair areas affected by SCC. The resistance to SCC by 12%Cr-5%Ni s is well-established in geothermal plants which have steam conditions much more severe than petrochemical plants.If the aforementioned material is applied as a weld overlay on discs damaged by SCC, it is expected to be more reliable than original low alloy steel base material.This paper also discusses the development and verification of weld overlays applied to rotors for SCC resistance.

SCC example for steam turbine rotor

Back ground

When boiler feed water and boiler water are treated with caustic chemicals (example; NaOH), the surfaces of the rotor surfaces, particularly in tight gaps, can accumulate corrosive materials in stages where transient wetness conditions exist. This zone is nominally defined as stages containing 2-6% wetness This accumulation can eventually lead to SCC cracks. In the present case, cracks were detected during PAUT inspection on the 9th stage T-slot roots of a steam turbine driving a process gas compressor. This rotor had been in operation for 8 years from 2001 to 2009 and the 9th stage disc resided in this transition zone. This rotor operation condition is given in Table I.

Table I. Steam Turbine Operating Conditions	
Steam Turbine Type	Extracting condensing turbine
Operating Speed	4000 RPM
Inlet Steam Temperature	500°C (932°F)
Exhaust Steam Temperature	50°C (122°F)
Inlet Steam Pressure	120 kgf/cm^2 (1700 psi)
Exhaust Steam Pressure	0.14 kgf/cm^2 (2 psi)
Rotor Material	Ni-1.25Cr-Mo-V forged steel, 11 stages (Figure1)

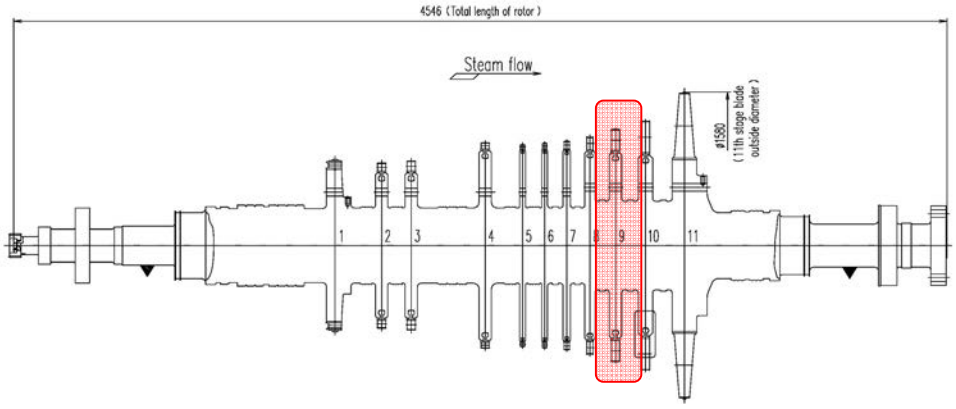

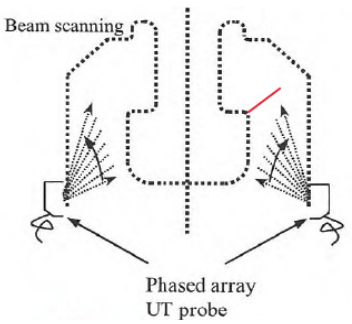

Investigation result

The damaged blade disc was cut into 8 test coupons and magnetic particle inspection (MT) was performed to verify the PAUT result. Fig.3 shows a representative coupon and Fig.4 shows the coupons after being split to expose the cracked areas on exhaust side of the root.. MT indications, shown in Fig. 5 & Fig. 6 matched the discontinuities found by PAUT in two locations on the 9th stage disc. This result verified the reliability of PAUT inspection.

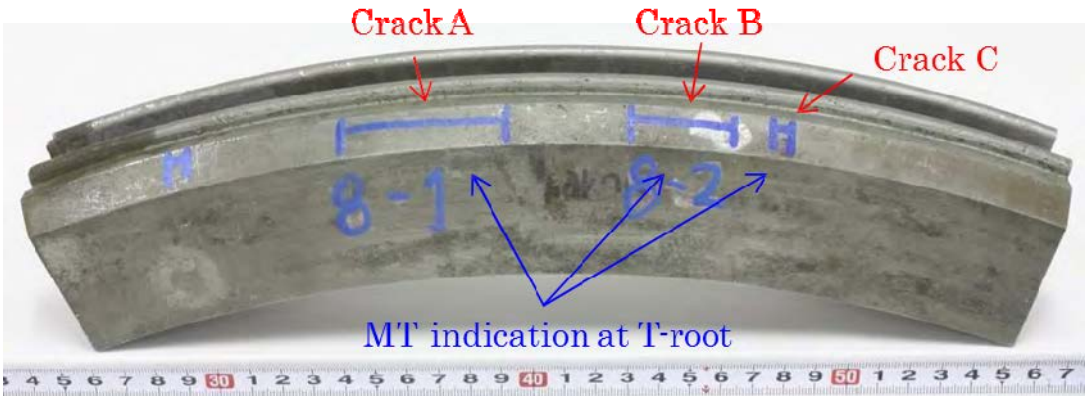

Fig 3 Overview of the cut disc (from exhaust side)

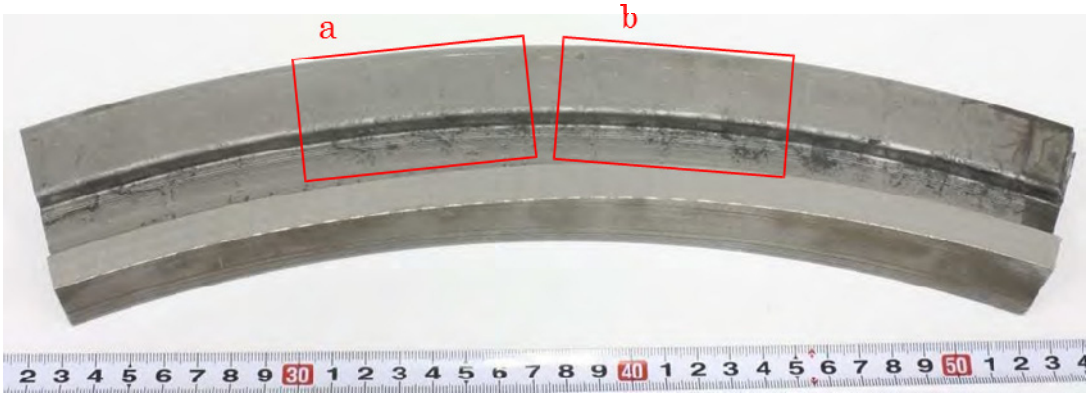

Fig.4 Overview of the split disc of the exhaust side

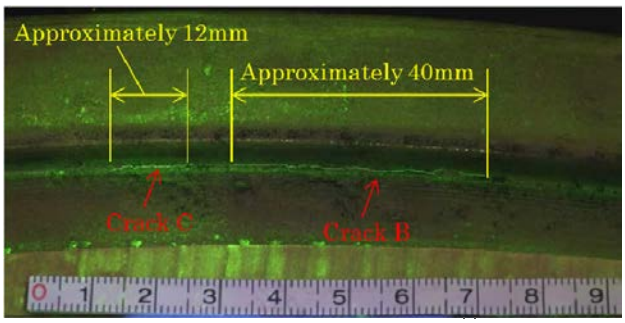

Fig.5 MT result of part “a”

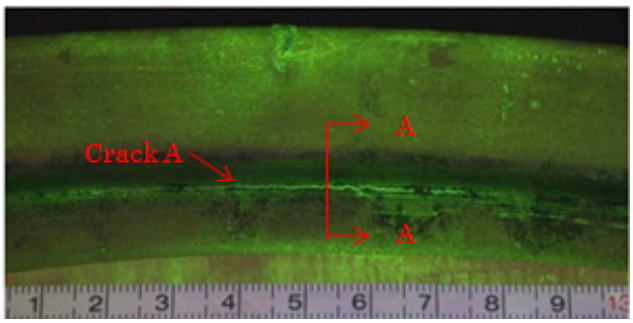

Fig.6 MT result of part “b”

After MT inspection, root cross section was examined by optical microscopy. The following results are found.

・The crack was found on the corner R of the disc groove where it is likely to be highest stress point. (See Fig.7)

・The crack had a jagged appearance, and exhibited crack branching, and scale within the crack. (See Fig 8.)

・Microhardness examination revealed no significant deviation in hardness (267 ~ 287HV) on adjacent to the crack compared to other areas (>248HV).

・The micro structure of this material was normal, tempered martensite.

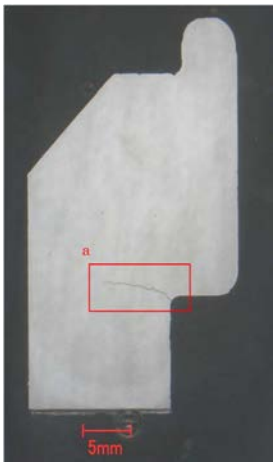

Fig.7 Section A-A on part B

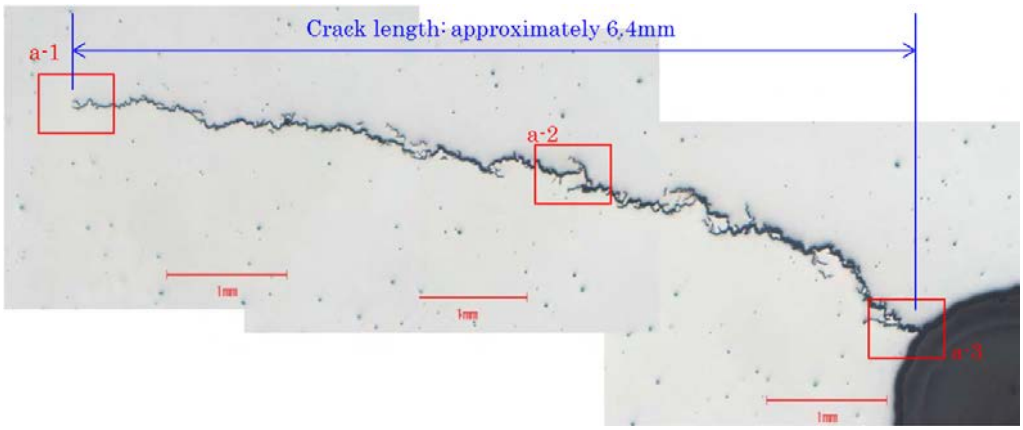

Fig.8 Magnified area of Fig 7 point “a”

Next, chemical analysis by Electron probe Micro-Analyzer (EPMA) was performed on the scale within the crack in order to confirm the existence of corrosive materials in the environment during crack growth.. As the result of this test, chlorine was detected throughout the crack. Analysis results are given in Table II.

Table II EPMA analysis results (wt%)

C	O	Al	Si	S	Cl	Ca	Cr	Mn	Fe	Ni	Cu
5.02	8.49	0.59	0.32	0.41	0.43	0.35	1.11	1.03	80.5	1.30	0.89

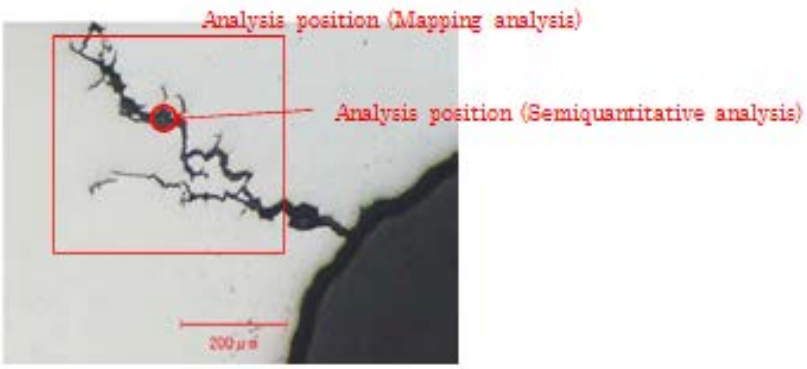

Fig.9 Section A-A on part B

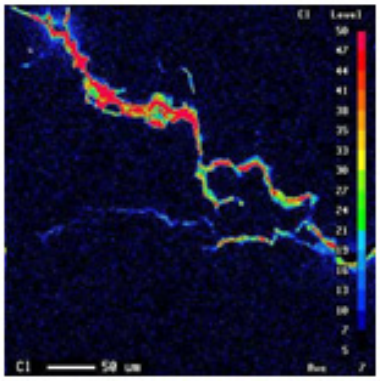

Fig.10 EPMA result of scale on crack

Additionally, the fracture surface was examined fractography study was carried out to identify Scanning Electron Microscope (SEM) on crack “B”. Fig. 11 shows the overview of this test sample and Fig.12 shows the SEM image of this result. As a result of this study, following results were found.

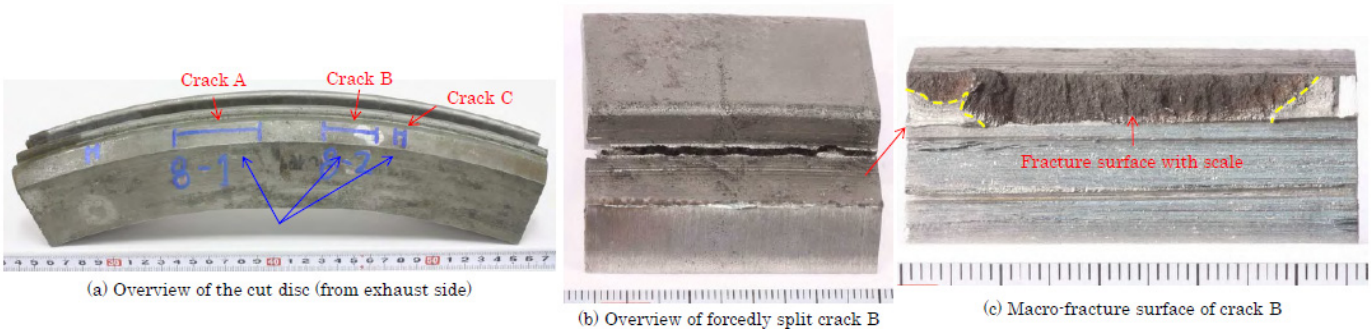

(a) Overview of the cut disc (from exhaust side)

(b) Overview of forcedly split crack B

(c) Macro-fracture surface of crack B

Fig.11 Overview of the split disc (Crack "B") of the exhaust side

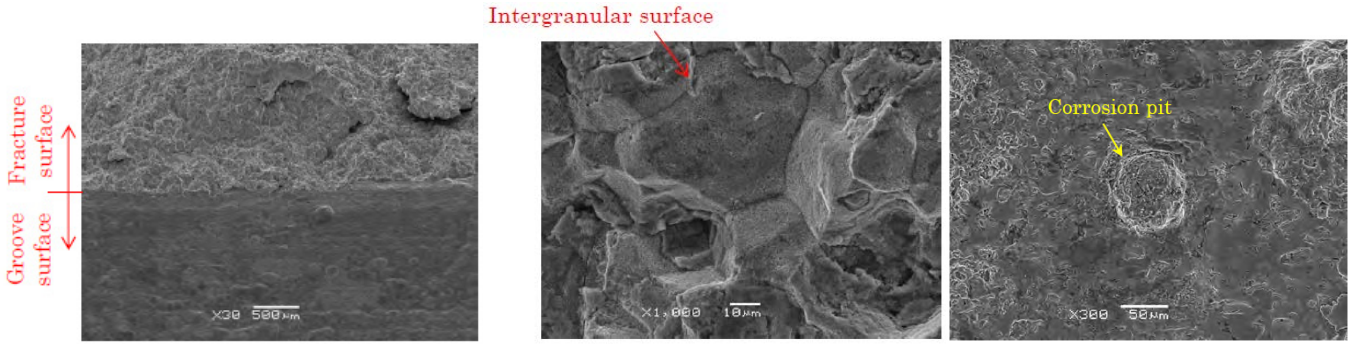

Fig.12 SEM image of fracture surface

・The whole surface on crack is covered by scale and this surface was relatively rough. It was found that the scale also contains about 6wt % chlorides by EMPA.

・Corrosion pits, ranging from 0.2 – 20μm were observed through the fracture surface.

・Intergranular fracture was the primary crack propagation mechanism.

The crack initiated at a corrosion pit approximately 50μm in depth.

Summary for this phenomenon

1) A Crack was observed on the corner R of groove where highest stress occurs and corrosive material(Chloride) was detected within the crack. Additionally, intergranular fracture, typical of SCC, was observed in fracture surface. Based on this information, the root cause was determined to be Stress Corrosion Fracture.

2) No striation pattern was observed. Low possibility of corrosion fatigue fracture.

3) Typical Root cause analysis is shown on Fig.13.

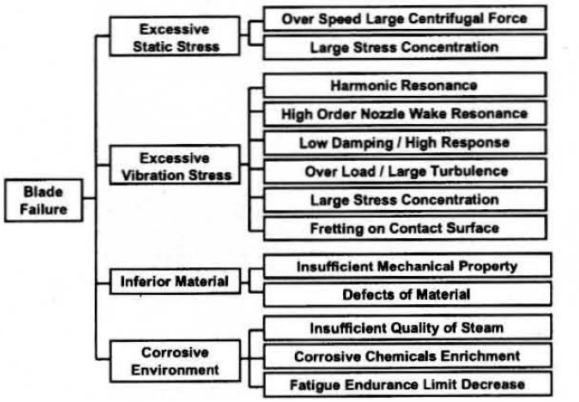

Fig. 13 Root cause analysis for rotor damage

Countermeasure for this phenomenon

1) The customer's decision to improve the rotor was based on the desire to have a reliable and and safely operating turbine. So, the root design was changed from circumferentially loaded T-slot root to an axial entry christmas tree roots, to reduce stresss and prevent accumulation of corrosive materials.
2) In order to change the root, the existing disc with crack was rebuilt by overlay welding.

Development of accurate life time estimation method for SCC

Back ground

Using a rotor made of 1.25NiCrMoV low alloy steel for its mechanical-drive steam turbine, Stress-corrosion cracks have been frequently observed in grooves of rotor blades exposed to wet and dry alternating conditions. Currently, crack growth rates are evaluated to calculate remaining turbine life and determine if it is remediation is required, or if the turbine may be used as-is for some period of time.

The equation (1) (EPRI Equation) has been commonly used to evaluate crack growth rates. Based on numerous blade damage data, the EPRI Equation was formulated by W. G. Clark[1)], et al. to evaluate apparent crack growth rates. In the past, the below equation has used for its evaluation in practice.

$$\ln\left(\frac{da}{dt}\right) = -4.968 - \frac{7302}{T} + 0.0278\sigma_y \qquad \ldots\ldots. (1)$$

$\frac{da}{dt}$: Crack growth rate (in/hr)

T : Temperature in Rankine scale (R)

σ_y : Yield strength of 0.2% (ksi)

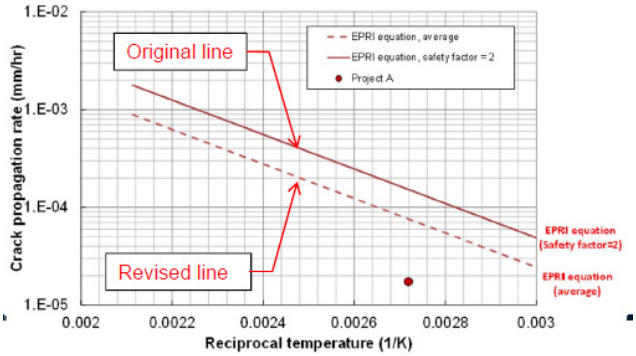

Fig.14 Comparison between MCO Experience and Evaluation by EPRI Equation

However, it has been often observed that the calculated crack growth rates are higher than the actual growth rates. For example, Table III shows the results of a previously-conducted evaluation.

Table III Calculated Residual Life Compared to Actual Life

	Continuous Operating Time (A)	Maximum allowable Crack Depth (b)	Crack Growth Rate (C)	Initial Crack Depth (D)	Estimated Residual Life	Total Lifetime
8th Stage	8 yrs	5.8 mm	1.5 mm/yr	1.9 mm	2.6 yrs	10.6 yrs
9th Stage	8 yrs	6.6 mm	1.0 mm/yr	5.9 mm	0.8 yrs	8.6 years

A crack was detected after eight years of continuous operation, and remaining turbine life was estimated from the length of a detected crack. The remaining turbine life, which was limited from the maximum allowable crack depth obtained from fracture toughness and the EPRI Equation, was estimated to be 2.6 years and 0.6 years, respectivelyand entire turbine lifetime calculated was 10.6 years and 8.6 years, respectively, for the 8th and 9th stage discs,. In many cases, our steam turbine rotors have operated without troubles for more than 15 years. Moreover, there are many examples in which the turbine is operated in very harsh conditions. This implies that the EPRI Equation can underestimate remaining turbine life. Also, a safety factory of 2 is usually applied whenever EPRI equation is used. However, this safety factor of 2 was not applied for the above evaluation. As shown in Fig. 14, the “Original line” represents the crack growth rate calculated with a safety factor of 2. The “revised line” shows the crack growth rate calculated without a safety factor of 2. The experience marked with the red dot in **Fig.14** indicates a lower crack growth rate than the revised line calculated without a safety factor. The findings imply that the EPRI Equation can underestimate remaining turbine life.

Comparison in Crack Growth Rates between EPRI Equation and MCO Turbine Conditions

The EPRI Equation is a formula that was empirically derived by field data collected from power plants and other facilities. So, a comparison in crack growth rates was made between MCO turbine material conditions and the EPRI Equation material conditions. This was done to study the possibility that the crack growth rates of MCO turbines are lower than those calculated from the EPRI Equation. **Table IV** shows the comparison results and literature experimental data[2)] of a crack growth rate for each turbine environment.

	MCO (Steam turbine for driving compressor)	EPRI (LP Steam turbine for Nuclear plant)
[illegible]	[illegible]	[illegible]
[illegible]	[illegible]	[illegible]
[illegible]	[illegible]	[illegible]
Crack propagation rate [m/sec]	Current = Using EPRI No field data including test result for MCO steam turbine	10^{-11} – 10^{-10} (Calculation from EPRI equation with safety factor 2 for MCO turbine condition; YS = 650MPa, 90 to 150℃)

Table.IV Comparison result

The empirical data of EPRI equation is based on materials and yield strength levels that are different from MCO turbine conditions.

Also, this empirical data was collected more than 30 years ago. Therefore, much of the data[3)] may not be relevant in modern turbine design as significant improvements have been made in terms of material cleanliness and root geometry. If crack growth rate is calculated by applying MCO turbine yield strength and temperatures to the EPRI Equation, the crack growth rate is approximately 10^{-5} m/s to 10^{-4} mm/hr , provided that the safety factor is two.

Work by Turnbull et al[2)] shows real actual crack growth rates of approximately 4.7×10^{-7} mm/hr for 3NiCrMoV steel with yield strength of 885 MPa (128 ksi). 1.25NiCrMoV has a significantly lower yield strength than the aforementioned material which reduces susceptibility to SCC. Furthermore,the operating speed limit, (which means centrifugal stress for blade), is also lower for this material. Considering the lower speed can further decrease the crack growth rate, it is possible that this material crack growth rate can be much lower than the experimental material value.

In summary, due to the conservative nature of the EPRI equation and given that MCO's turbine materials and conditions may not closely match power generation conditions, it was necessary to perform testing to determine actual crack growth rates for 1.25NiCroMoV steels to more accurately predict residual life of rotors.

Evaluation Method of Crack Growth Rates

SCC can be simulated with notched specimens which are then partially fractured to initiate a crack. Then, a constant load is applied by wedging open the crack. The specimens are then submersed in an environment conducive to SCC and held for a period of time to allow the crack to propagate. Crack growth rates can most simply be determined by subtracting the crack length before and after testing, and dividing by the time of the test. However, this method assumes uniform crack growth rates. Therefore, in addition to this method, the Potential Drop Method (PDM) was utilized to measure in-situ crack tip velocities as determined by a change in electrical resistance of the crack test (CT) specimen. Fig. 15 shows the conceptual illustration of PDM. However, it is necessary to finally obtain a crack growth rate from post-testing fracture surface analysis for correction.

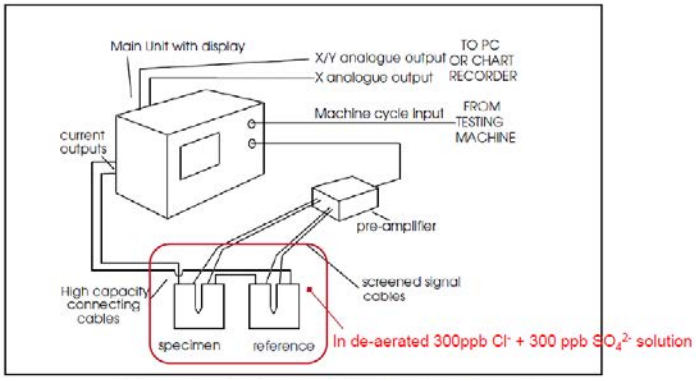

Fig.15 Schematic diagram of PDM equipment

Table V. Test Conditions for SCC Growth Rate Testing	
Material	1.25NiCrMoV Steel
Solution Chemistry	100 ppb or 300 ppb Cl^- + 100 ppb or 300 ppb SO_4^{2-}, de-aerated
Solution pH	7 (neutral)
Applied Stress*	
Test Temperature	120°C (248°F)
**two specimens for each stress intensity factor listed*	

Test Result

In this test, cracks did not grow at 30 MPa√m and 40MPa√m within the measurement time. When a stress intensity factor was increased to 50 MPa√m, cracks grew in both specimens at a constant rate. In case of 90MPa√m, Crack growth tendency was seen in two specimens approximately 700 hours after the start of the test and crack growth rate is faster than the case with 50 MPa√m . Fig.16 shows the result of K=90MPa√m case.

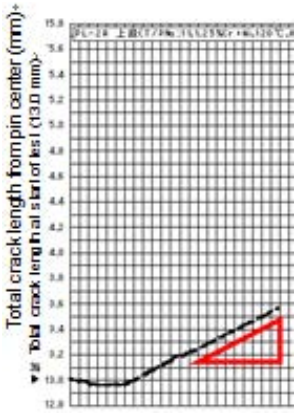

Fig.16 Result of K=90MPa√m

Summary of All Test Results

Test results are shown in Fig.17. As noted in Fig.17, the blue dots show the test data for each test case and black dotted line shows the actual expected crack growth rate. Also shown is the crack growth rate calculated from the EPRI equation at yield strength of 773 MPa (112 ksi) and a test temperature of 120°C as indicated by the brown dotted line. Within the test duration, there was no crack growth in K=30 and 40MPa√m.Technically, the crack growth rate for these conditions can be measured if the test continues longer. However, a limit rates mechanically obtained from the detection limit of PDM within test operation time in order to assume the limit rate.

In this Figure, it is evident that crack growth rates depend on stress intensity factors. Ccrack growth rate is very slow in the low stress intensity range. On the other hand, for K≥50 MPa√m, a crack growth rates increaseby more than one order of magnitude compared to the low K values.
Furthermore, the crack growth rate on actual data is faster than that obtained from the EPRI Equation in the range of high stress intensity over 50MPa√m.

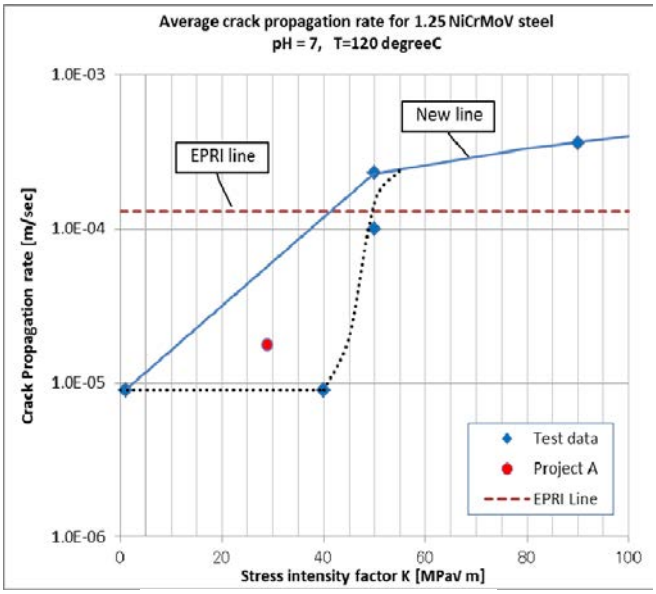

Fig.17 Summary of all test data

For K≤40MPa√m, the crack grow rate on project "A" which was measured at site is relatively close to the test data. The blue solid line in Figure 17shows the test data with a safety factor of 2 in order to account for a variety of operating conditions. In this line, the crack growth rate is divided into Stage I (low stress region) and Stage II (High stress region) and it can describe as the below equation.

$$T=\int_0^T dt = \underbrace{\int_{a1}^{a2} \frac{da}{C1\times exp^{C2*K_{(a)}}}}_{\text{Stage I}} + \underbrace{\int_{a2}^{a3} \frac{da}{C3\times K_{(a)}{}^{m}}}_{\text{Stage II}}$$

a1: Initial crack depth
a2: Crack length @K_I=50MPaVm
a3: Allowable Crack depth

This result not only improves the accuracy of life time estimation but also covers the actual measurement data with blue solid line. Although the life time in high stress intensity region is shorter than predicted by EPRI, low stress intensities can be safely operated longer than recommended by EPRI.

In MCO statistical data shown in Fig.18, the percent of stress intensity factors less than K=40MPa√m comprises approximately 70 percent of rotors which exhibited SCC damage found byPAUT inspection.
The life of many rotors can be extended because of the new method and rotor replacement can be offered at proper and precise timing with this method.

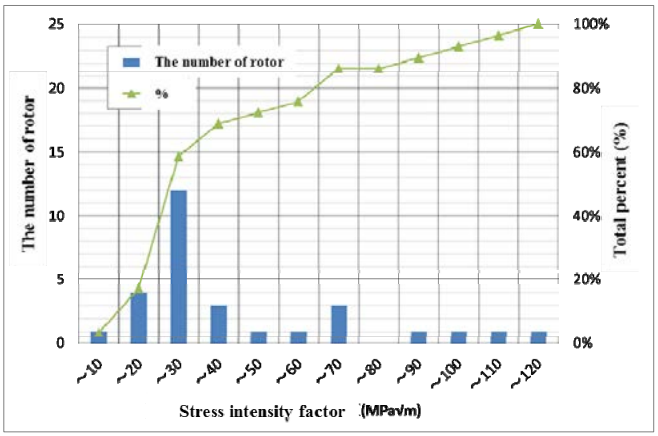

Fig.18 Statistical data for K value by PAUT inspection

Development of welding method of new rotor material with SCC resistance

Typical welding repair for rotor

SCC is the result of a combination of three factors – a susceptible material, exposure to a corrosive environment, and tensile stresses above a threshold. If any one of these factors are eliminated.

Risk of SCC can be reduced significantly by reducing the stress in the blade root. In this approch, axial entry roots offer several advantages to their radial entry counterparts. Radial entry blades do not present a surface to react tangential loads, so a twist-lock style blade cannot be used. They also rely on pack compression in order lock the blades in position. The design also is not open to steam flow which allows for localized accumulation of corrosive contaminants. Finally, the "closed" nature of the design makes inspection difficult, if not impossible. Axial entry roots provide an answer to each of these design difficulties. Additionally, axial entry root designs with christmas type reduce radial stresses 30-50% over the conventional design.

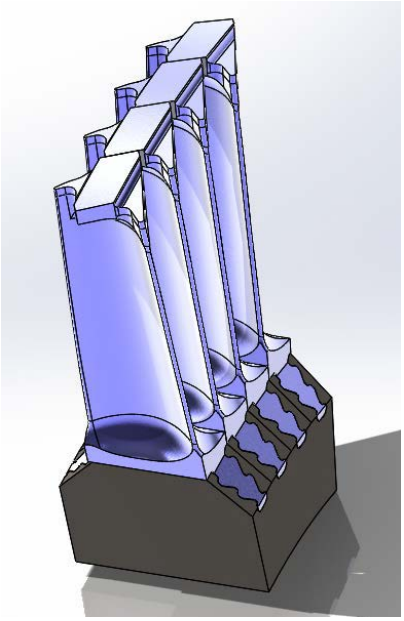

Fig 19 Upgrade blade design for replacement

In order to change the root, the existing discs have to be rebuilt weld repair. To qualify the welding procedure,, welding parameters are chosen based on the chemical composition of the rotor, and a post-weld heat treat (PWHT) is developed that can achieve desired properties through the base metal, heat-affected zone (HAZ) and weld material.

The Larson-Miller Parameter is a dimensionless factor that combines the effects of time and temperature on a material, is often used to determine a PWHT condition. Based on the hardness results and required strength, a target Larson-Miller Parameter for the actual weld will be chosen as shown in Fig. 21, and mechanical properites are verified in full-scale weld tests.

After successful qualification, the rotor is prepared for welding by machining off the existing discs. Care is taken to establish reference radial bands to ensure that no significant distortion or bowing occurred during welding or stress relief heat treatments. After welding, the discs are rough-machined and thoroughly inspected for cracks or other flaws by ultrasonic inspection (UT) and magnetic particle inspection (MT). The rotor is then post-weld heat treated to relieve welding stresses and temper the material in the same manner as the test piece. Finally, the new discs are machined into their new shape as shown in Figure 20, and axial-entry roots are cut. New blades are installed and the rotor is at-speed balanced.

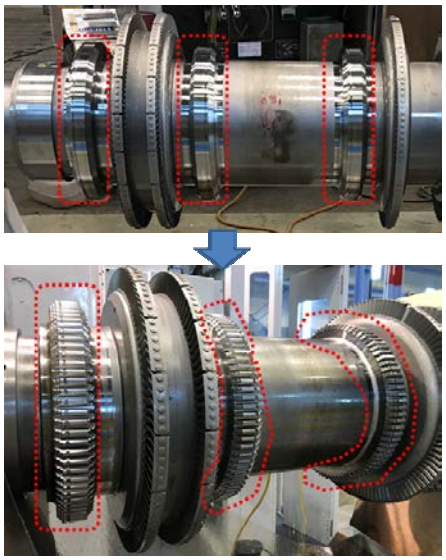

Figure 21
Before and After for welded rotor

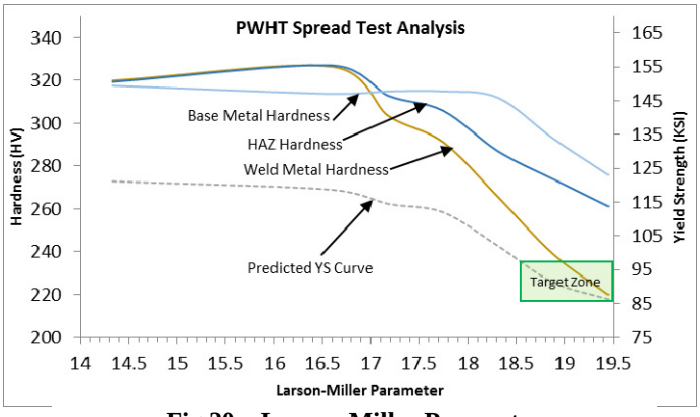

Fig 20 Larson-Miller Parameter
(For material equivalent with AISI4350)

High corrosion resistance material for turbine rotor

Another option to eliminate the risk of SCC is applying a new material with high corrosion resistance.. Although the improvement of purity for water is recommended to end user, steam chemistry control can be difficult. In geothermal plants, geothermal steam contains large quantities of chloride, sulfate, hydrogen sulfide, carbon dioxide, and other such corrosive chemicals. The corrosive substances contained in the steam are 100 to 1,000 times more plentiful than in steam turbines for fossil fuel power plants where the feed water has been chemically treated. 12%Cr-5%Ni steel has been developed for steam turbines to withstand such steam environments. This rotor material composition is shown in Table VI. Many laboratory tests as well as decades of reliable service have confirmed its resistance to severe steam environments.

Material		12%Cr-5%Ni rotor	1.25NiCrMoV Conventional
Mechanical property	0.2%Yield strength (MPa)	≧ 635	≧ 638
	Tensile strength (MPa)	≧ 740	≧ 785
	Elongation (%)	≧ 16	≧ 15
	Reduction of area (%)	≧ 45	≧ 40
	Absorption energy (J)	≧ 90	≧ 39.3
	50% FATT	≦ 40	<40
Chemical Component (wt%)	C	≦ 0.06	0.25 ~ 0.33
	Mn	≦ 1.0	0.35 ~ 0.65
	P	≦ 0.015	≦ 0.015
	S	≦ 0.005	≦ 0.015
	Si	≦ 0.30	0.15 ~ 0.35
	Ni	5.0 ~ 5.5	1.00 ~ 1.50
	Cr	11.5 ~ 12.5	1.00 ~ 1.50
	Mo	0.8 ~ 1.2	0.40 ~ 0.60
	V	≦ 0.1	0.05 ~ 0.15
Field service		For geothermal power plant	For chemical plant

Table VI. Comparison Table for Material composition

Although 12%Cr-5%Ni steel rotor has high corrosion resistance and similar strength to conventional heat resisting rotor steels, the derating of mechanical properties above 400°C (752°F) is higher than compared to conventional rotor alloys one as shown in Fig.22. (Green line VS Redline). Therefore, this material is not suitable for all stages of a steam turbine for chemical plants with steam temperatures over 500 °C (932°F).

However, SCC is only problematic in stages which contain 2 to 6 % wetness (Transition Zone) where steam temperatures are typically <200°C (<392°F) Accordingly, while this material is not suitable for HP sections, it can be very useful for LP section discs.

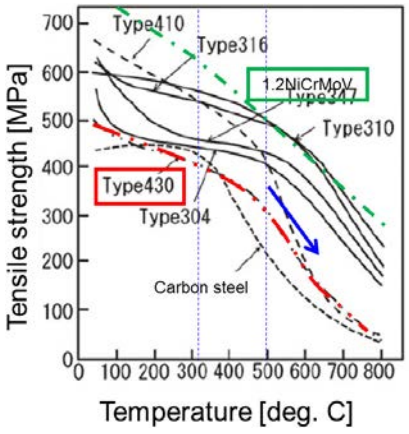

Fig. 22
Tensile stress VS temperature

Welding repair with high corrosion resistance material for rotor

For one chemical plant, the compressor drive steam turbine rotor experienced blade root failure by SCC due to excess NaOH in the steam. I The most advisable approach to preventing future failures is to control steam chemistry o keep low level of corrosive materials such as sodium (Na) and chlorine (Cl).
However, in the event steam chemistry cannot be controlled to OEM recommended levels, materials susceptible to corrosion damage can be replaced with high corrosion resistant alloys.
12%Cr-5%Ni steel was investigated for resistance to the subject environment.

As previously mentioned, Larson-Miller Parameter (LMP) was used to determine a PWHT condition in order to establish the weld repair techniquefor this material. Bothoth materials have a different material composition, so the issue is to develp the technology which acheives both the desired hardenss of HAZ area and the strength after welding. In order to reduce the hardeness in the HAZ less than 350 HV, some trial welds were performed with a range of PWHT conditions. In case over 350HV, it is said that the risk of crak on weld will be significantly increased. For 12%Cr-5%Ni steel, it is already found that 580 degree C x 10Hrs is the best condition to keep the required strength and proper hardness. Meanwhile, conventional material (1.25NiCrMoV) needs over 600 degree C x 10Hrs in order to reduce the hardness of HAZ area. So, two steps of welding repair was recommended to achieve the target (TS>785MPa, Hardness of HAZ area <350HV.)

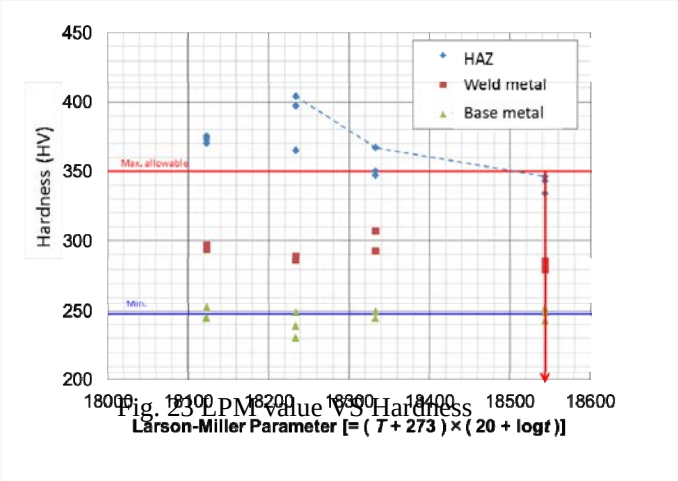

Fig. 23 LPM value VS Hardness

As shown in Fig.23, LMP value over 18500 is required to reduce the hardenss at HAZ less than 350HV. So, as first step, PWHT at 610 degree C x 8.1 Hrs is performed after a few layers welded. Then, PWHT at 580 degree C x 10 Hrs is performed after completion of all layers welded. (Although the hardness of base metal is less than the minimum value 250HV, the hardness before PWHT was not changed after PWHT and found the low sensitiveness within these heat treatment conditions.) With this procedure, LMP values will be over 18500 and achives both the required strength and proper hardness at HAZ.

After successful qualification for this welding technique, SCC tests for this welding material were carried out in order to verify the effectiveness under excess amount of NaOH condition. The exposure of U bend specimens in liquid of 35% NaOH aqueous solution was found to be most fitted for this purpose in past SCC result for low carbon steel under NaOH condition in Fig.24 and Fig.25.

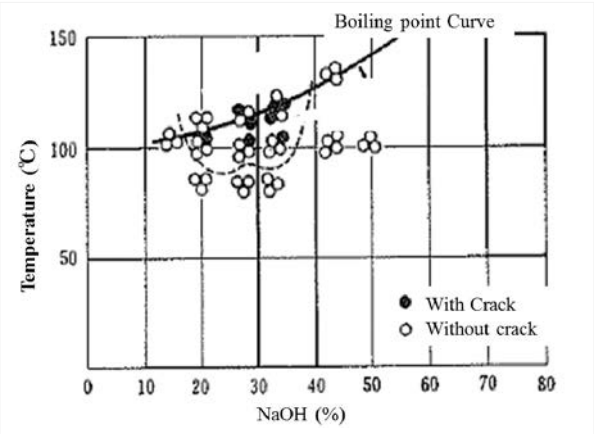

Fig. 25 SCC test result
for low carbon steel under NaOH solution

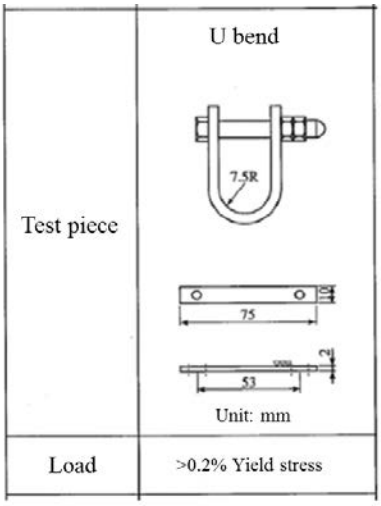

Fig.24 U bend specimen for SCC test

The results, given in Table VII compare the time to initiate cracks relatively between conventional material and 12%Cr-5%Ni steel in NaOH condition. The test condition was set as shown in Table 5 and test results are shown in Fig.25.

No	Material	Solution	Temperature	Time	Note
A	12%Cr-5%Ni steel	35%NaOH	120℃	50hrs 100hrs 1000hrs	With 30g/L PbO for acceleration
B	1.25NiCrMoV Steel				
C	12%Cr-5%Ni steel Weld metal				

Table.5 Test condition for SCC test

Under this environent, cracking was first observed after occurred after 100 hours in the conventional rotor material.
On the other hand, 12%Cr-5%Ni steel forging material (Test piece A & C) and weld metal made by aforementioned PQR did not crack after 1000 hours in the same environment.
Therefore, the corrosion resistance for 35%NaOH for 12%Cr-5%Ni steel improved relatively ten times as long as conventional material and good performance was verified on this test.

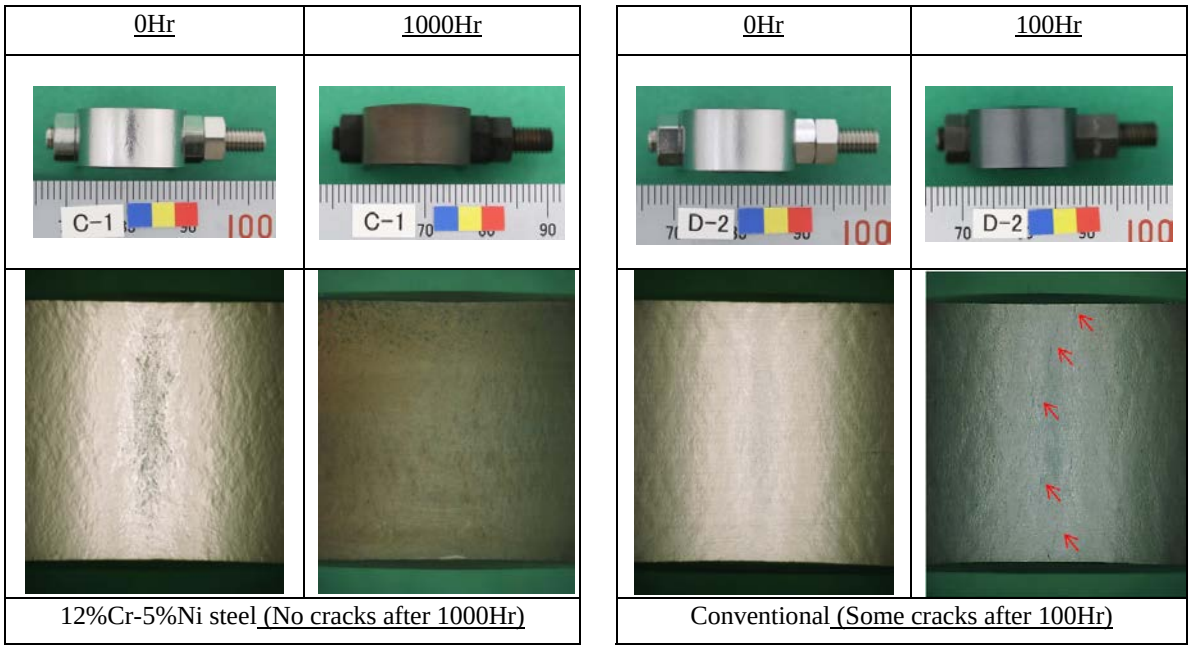

Figure 26 Test result of U bend test under 35% NaOH condition

As a result of this test, and the welding technique to apply 12%Cr-5%Ni overlay on conventional rotor discs was validated as suitable for for service in severe environments.

Conclusion

For typical SCC issues, the proposed life time estimation can help the end user to consider the proper replacement timing of damaged rotor and it could improve the accuracy of that verification.
Additionally, overlaying weld buildup of cracked damaged discs with corrosion resistant material can improve the life of the rotor beyond the predicted life of the original material. Due to the differences in tempering requirements for the two materials, a two-step PWHT process is applied to achieve the balance of hardness at HAZ and strength of base metal.

NOMENCLATURE

MT	Magnetic Particle Test
PAUT	Phased Arrayed Ultra Sonic Test
K	Stress intensity factor (MPa √m)
C1,C2,C3	Material constant number by experiment
PWHT	Post weld heat treatment

REFERENCES

(1) W. J. Clark, Jr., B. B. Seth, and D. H. Shaffer, ASME 81-JPGC-Pwr-31 (1981)

(2) A. Turnbull, Corrosion Vol. 64, No. 5, pp.420 (2008)

(3) EPRI Report NP-2429, Vol. 2, (1982)

(4) Japan Nuclear Energy Safety Organization, Heisei ninenndo nikkerukigokin ouryoku fushokuware sintenhyoka gijutujisyo ni kansuru hokokusho [FY2011 report on technical demonstration for evaluation of stress-corrosion crack growth in nickel base alloy] (2011)

(5) R. Kawabata, and E. Yanagisawa, Engineering document of Structure No. 1 Laboratory, Strength Research Department, Structure No. 1 Laboratory 1500992 (2016)

(6) H. Matsumura, H. Fujii, T. Yoshioka, T. Endo, H. Itoh, and T. Tsuruta, International Symposium Fontevraud II, pp.588 (1990)

(7) Y. Ishibashi, Y. Maebashi, K. Sato, and S. Zenitani, Engineering document of Material No. 2 Laboratory, Material Research Department, Material No. 2 Laboratory 1700050 (2017)

(8) A. Turnbull, and S. Zhow, NACE CORROSION 2010, No.10288 (2010)

(9) H. Ito, Zairyo-to-kankyo: Corrosion engineering, Vol. 50, pp.564 (2001)

(10) T. Hattori, et al, Strength Design Handbook for Failure Prevention of Products NTS, p.327 (2012)

(11) Y. Ishibashi, S. Zenitani, and Y. Konno, Engineering document of Material No. 2 Laboratory, Material Research Department, Material No. 2 Laboratory 1500475 (2016)

(12) Y. Maebashi, and K. Sato, Engineering document of Chemical No. 3 Laboratory, Chemical Research Department, Chemical No. 3 Laboratory 1600456 (2016)

(13) Y. Maebashi, and K. Sato, Engineering document of Chemical No. 3 Laboratory, Chemical Research Department, Chemical No. 3 Laboratory 1600919 (2017)

(14) Y. Maebashi, and K. Sato, Engineering document of Chemical No. 3 Laboratory, Chemical Research Department, Chemical No. 3 Laboratory 1700220, (2017)

ACKNOWLEDGEMENTS

The authors wish to thank all involved colleagues from MCO and ****** for the technical assistance and the precious feedback